Neuronal Oscillations on Evolving Networks: analysis and extensions

Felipe Duque Quiceno, Balazs Nyiro, Isabelle Ogland and Jie Gan

Abstract

Brain networks in Neurodegenerative diseases such as Alzheimer's display distinctive forms of structural damage as the disorder progresses over time. These network alterations may underpin some of the wide ranging cognitive symptoms of Alzheimer's. This work extends previous attempts to model the underlying biological processes of the disease, including the aggregation and cascade of toxic proteins and their impact across the brain connectome. We expand prior research showing other implications of long term disease progression on the connectome, by modeling the topological evolution of the network and it's relationship with cognition, as well as the role of myelin thickness and the effect of increased signal delays on cognitive deterioration.

Introduction: the biology of Alzheimer's disease

Neurodegenerative diseases are a class of disorders which are associated with the progressive damage or death of neurons, one of which is Alzheimers disorder (AD). Alzheimer's is the most frequent cause of dementia [1], and is associated with symptoms such as memory loss, reduced cognitive functioning and behavioral changes. Considering AD affects approximately 50 million people worldwide, and these numbers are only set to increase with aging populations [2], understanding the mechanisms of AD in order to develop treatments and preventative measures is of great interest from a global health perspective.

The development of AD is thought to be strongly linked to substantial accumulations of toxic proteins in the brain. These toxins take the form of misfolded and altered proteins inside neurons, specifically excessive phosphorylation of tau protein which leads to neurofibrillary tangles, and beta-amyloid proteins outside of neurons, associated with senile plaques [3]. These toxins are problematic as they are thought to hinder normal brain processes and lead to maladaptive nerve cell changes, as well as resulting reduction in neural connections and general brain atrophy. A more detailed explanation of these neurodegenerative processes are shown in Figure 1.

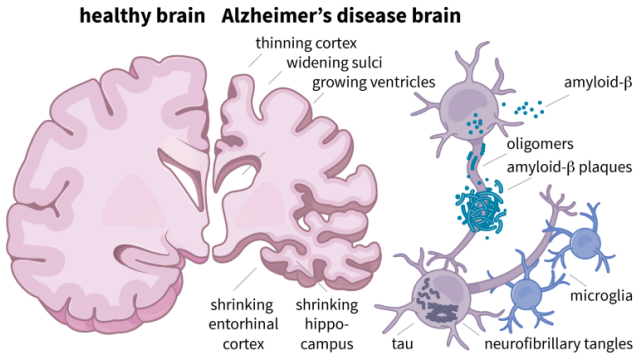

Fig. 1. Illustration of Neuropathology in Alzheimer's disease. Amyloid precursor proteins generate amyloid-β peptides, which form flexible soluble oligomers, that accumulate to become amyloid-β plaques. These plaques hinder neural processes, and prompt microglial activation as well as neuroinflammation. Within the neurons, neurofirbillary tangles are created from hyperphosphorylated tau proteins, these tangles take the place of organelles and interfere with vesicular transport. The death of neurons leads to brain atrophy, particularly density reduction in the cerebral cortex, an increase in the width of the cortical sulci and size of the ventricles, and reduced size and volume of the hippocampus and entorihnal cortex. The cognitive deficiencies related to AD are therefore largely associated with the consequences of brain atrophy and related outcomes. Taken from [4].

The atrophy of certain temporal lobe structures such as the hippocampus and entorhinal cortex shown in Figure 1, has further damaging consequences from a network perspective. These regions are thought to be particularly important for information flow, therefore damage to these regions not only

impacts localised functioning but also may affect connections that enable communication and integration across lobes. This means that not only is memory consolidation for instance reduced by impairment in the hippocampal circuitry, but also wider information integration across lobes more generally, including the frontal cortex.

Presently much is known about the biological markers of AD, less so the pattern of progression and network dynamics. In this paper, we reproduce and extend work by Goriely and colleagues [5] showing the predictive role of network degradation on cognitive decline.

Network model of neurodegenerative diseases

Considering the challenges of clinical AD experiments to understand the cascade of pathology, computational models provide alternative methods that give insights to the potential progression of the disease as well as a better understanding of its processes. Network models, are a particularly useful tool for simulating the brain connectivity changes between a healthy and diseased brain. Such models, represent the brain as a graph, where each node is a collection of neighbouring neurons and the edges represent the physical connection between brain regions. Neurodegenerative diseases, can then be modelled by modifying the graph's edges or nodes, following a specific set of dynamics representative of the disease.

Early symptoms of AD include impaired olfaction, processing of spatial information, and storage of information in memory [6]. Gamma oscillations (Gamma = [30,100] Hz), also show a slow decrease in activity in AD patients, and are thought to play an essential role in encoding the transfer of information between different brain regions [7]. Therefore, some reasonable markers of an AD model's performance, are the behaviour of the nodes in the gamma region over time, and the dynamics of brain lobes' activity.

Goriely and colleagues's [5] model, recreated in this report, aims to explain known AD symptoms as the effect of increasing toxic protein concentration over long time spans (30 years). Disease progression is simulated over a slow time scale (years), while its symptoms are simulated in short *snapshots* of 10 seconds along several years. In this report we will first simulate the neural network structure in an initially healthy brain, and then simulate the changes in its structure (and its effects) as a result of modifying the network's connection weights (edges).

According to the description of Goriely, et al. [5], network edges are represented by a symmetric matrix ($\mathbf{W} = w_{kj},\ k,j \in \{1,...,N\}$), where w_{kj} is the ratio of the number of fibers to the mean fiber length between the k-th and j-th nodes. Based on this, we compute the weighted Laplacian matrix $\mathbf{L} = \rho(\mathbf{D} - \mathbf{W})$ where the transport duration is given by the overall velocity constant ρ. The initial weights ($\mathbf{W}(0)$) and overall network's structure used, come from the Budapest Reference Connectome 3.0 [8], which contains a total of 83 nodes from 7 different brain regions.

The concentration of toxic proteins inside a node is given by the discretized form of the Fisher-Kolmogorov-Petrovsky-Psikunov equation [9] (Equation (1)), where α is the rate of protein conversion from healthy to toxic. The initial conditions as per [5] are $c_k(0) = 0$ for all k, except $c_{26,68}(0) = 0.025$. Given that nodes 26 and 68 are located in the hippocampus, equation (1)'s initial conditions are set, so that the modelled disease manifests itself in the limbic region first as is known to occur in the real counterpart.

$$\dot{c}_k = -\sum_{j=1}^{N} L_{kj} c_j + \alpha c_k (1 - c_k), \qquad (1)$$

The deposited amyloid beta and tau proteins inhibit signal transduction at synapses and can also lead to cell death by blocking cellular metabolism. Over time, the extent of damage to the network is given on a scale of zero to one ($q_k \in [0,1]$) where 0 is healthy and 1 is the maximum damage value, with a dynamic determined by equation (2). The damage of each node over time is a monotonic function, whose speed is proportional to the node's concentration of toxic proteins.

$$\dot{q}_k = \beta c_k (1 - q_k) \qquad (2)$$

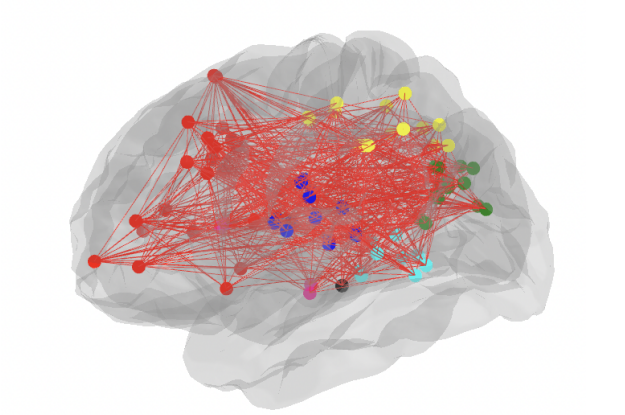

Fig. 2. Visual representation of the brain network, using Budapest Reference Connectome 3.0 nodes and weights. The different node colors represent the brain region they belong to. Red: Frontal, Yellow: Parietal, Green: Occipital, Aqua: Temporal, Pink: Limbic, Blue: basal ganglia, Black: Brain Stem

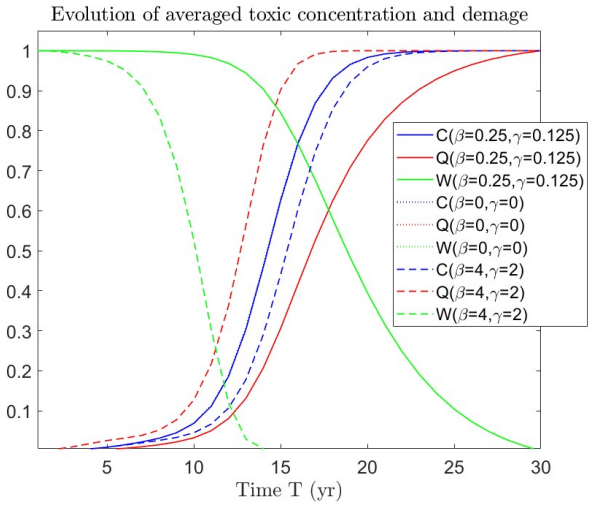

Fig. 3. Evolution of averaged toxic concentration and damage. Solid lines indicates the real values and the dashed and dotted lines indicate the unreal –exaggerated– values. In all cases, the toxic proteins (and with them the extent of damage) start to increase strongly between the tenth and fifteenth year.

β is the toxic proteins' strength. It determines how much effect the toxic proteins have on the speed of damage development.

As mentioned above, damage to cells impedes the flow of substances, and because of the networked nature of the system, damage to individual nodes affects those in contact with them. Connection strength between nodes is modelled to decrease monotonically, proportional to the total damage between the interacting nodes (Equation (3)),

$$\dot{w}_{kj} = -\gamma w_{kj}(q_k + q_j) \qquad (3)$$

Where γ is the relative rate of change. The previous three equations are solved as a closed system of ordinary differential equations using Matlab's ODE45 function.

The speed of the damage

Three biomarkers were used to describe the extent and rate of network damage: The average concentration of toxic proteins $C(T) = (1/N)\sum_{j=1}^{N} c_j(T)$, the average damage $Q(T) = (1/N)\sum_{j=1}^{N} q_j(T)$ and the scaled average weight $W(T) = ||\mathbf{W}(T)||/||\mathbf{W}(0)||$, where $||\mathbf{W}|| = N^{-2}\sum_{kj=1}^{N} w_{kj}$. $C(T)$ and $Q(T)$ clearly varied at the same rate and to the same extent. Since these amyloid proteins are not transported in the system, the process is characterized by a non-linear run-up and it is not significantly slowed down by the damage in the network until the whole system reaches a maximum level of degradation around the 15 to 20 year mark (Figure 3). If we look at this process for each brain region (Figure 4), we can see that the damage starts in the limbic region, but quickly spreads to other brain areas where the same degree of damage is observed in later years.

In contrast, for $W(T)$ we see that, while for realistic parameter values there is a lower degeneration rate (which reaches its minimum by the 30th year), for unrealistically high values this happens already by the 15th year, meaning that the network edges' dynamics are more sensitive to parameter variation than the toxic protein concentration and the node damage dynamics (Figure 3).

Resting-state brain dynamics

So far, our analysis has focused on the longitudinal changes in the brain structure over an individual's lifespan. We turn our attention now to analysing the behaviour of the brain at a fixed timestamp, by analysing the *resting-state dynamics*. That is, for a given year T, we hold the brain network $W(T)$ fixed and simulate a dynamical process of brain activity until a steady state is reached. By analysing the properties of this steady state (in terms of, for example, the size

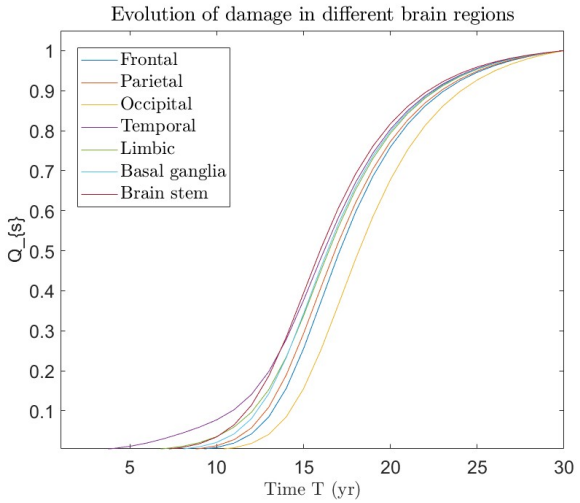

Fig. 4. Evolution of damage in different brain regions. Although initially, toxic proteins were only present in the limbic region, damage spreads over the entire cortex, affecting nodes of all other regions in around 15 years from damage onset. Occipital lobe is the last to get affected, but finally develops the same damage as the rest of the brain.

and variation in oscillatory activity), we get some sense of how brain functioning might qualitatively change at each time step.

In the study, a simple neural-mass model is used where each node in the brain network represents a large interacting excitatory and inhibitory neural population. For each node k, we represent the combined excitatory and inhibitory neural activity with the complex number $z_k \in \mathbb{C}$, where the real part represents excitatory activity and the imaginary part the inhibitory activity.

Let us first consider the dynamics at a given node in isolation (i.e. as if it was disconnected from the whole network). The paper proposes the following independent dynamics:

$$\dot{z_k} = F(z_k) = z_k(\lambda + i\omega_k - |z_k^2|) \qquad (4)$$

The parameters are as follows. $\lambda = -0.01$ represents a decay term. Next is an intrinsic frequency $\omega_k = \omega + \delta_k = 40/2\pi + \delta_k$ rad/s, where $\delta_k \sim \mathcal{N}(0, 0.1)$. The i represents the imaginary unit and $|z|$ is the absolute value of a complex number. This model presents a Hopf bifurcation when $\lambda > 0$, with stable oscillations of angular frequency ω_k.

Next, we add the "network dynamics", which allows the excitatory neurons from regions to influence one another via the network $W(T)$:

$$\dot{z}_k = F(z_k) + \kappa S\left(\Re\left(\sum_{j=1}^{N} w_{kj} z_j(t - \tau_{kj})\right)\right) \qquad (5)$$

The parameter $\kappa = 10$ modulates the coupling strength, and $S(x) = 1/[1+\exp(-x)]$ represents the sigmoid function (ensuring that the input from other neurons is bounded between 0 and 1). The Real operator $\Re$ ensures that only the real part is taken from other nodes' activity, which means that the excitatory part is the only influence between brain regions. Mathematically, the model is designed so that when isolated from the rest of the network, each node would present an oscillatory activity steadily declining towards zero with frequency 40 Hz ($F(z_k)$), and go over the Hopf bifurcation and stabilise at an oscillatory state when connected to the rest of the nodes.

Finally, note the differential equation is in a delay differential form: $z_j(t-\tau_{kj})$ ensures that there is a time lag of duration τ_{kj} before the activity at node k impacts node j. This time lag is determined from the distance between the nodes - the fiber length is taken and divided through with a mean signal speed of 150 cm/s, resulting in delays that tend to occur in the order of 130 ms (this is arguably slower than we might expect, but changing the order of magnitude closer to a realistic 30 ms resulted in very different results, so we stuck with the 130 ms we arrived at by following the instructions in the paper [5]).

In order to simulate these dynamics we initialised with random initial states z_k drawn from a normal distribution over the real and imaginary parts both of mean of 0 and variance of 1. The simulation was run initially for 3 seconds to allow the nodes to settle into a regular oscillating pattern, followed by 10 seconds of simulation used for the results.

In Figure 5, we visualise some of these results. For $T = 7$, we show the excitatory and inhibitory behaviour of two arbitrary nodes (60 and 3). Node 60 is well-connected to a number of neighbours, and we can see it maintains oscillatory activity throughout the simulated period. On the other hand, Node 3 is isolated and as expected the oscillations decay. In the bottom left, we

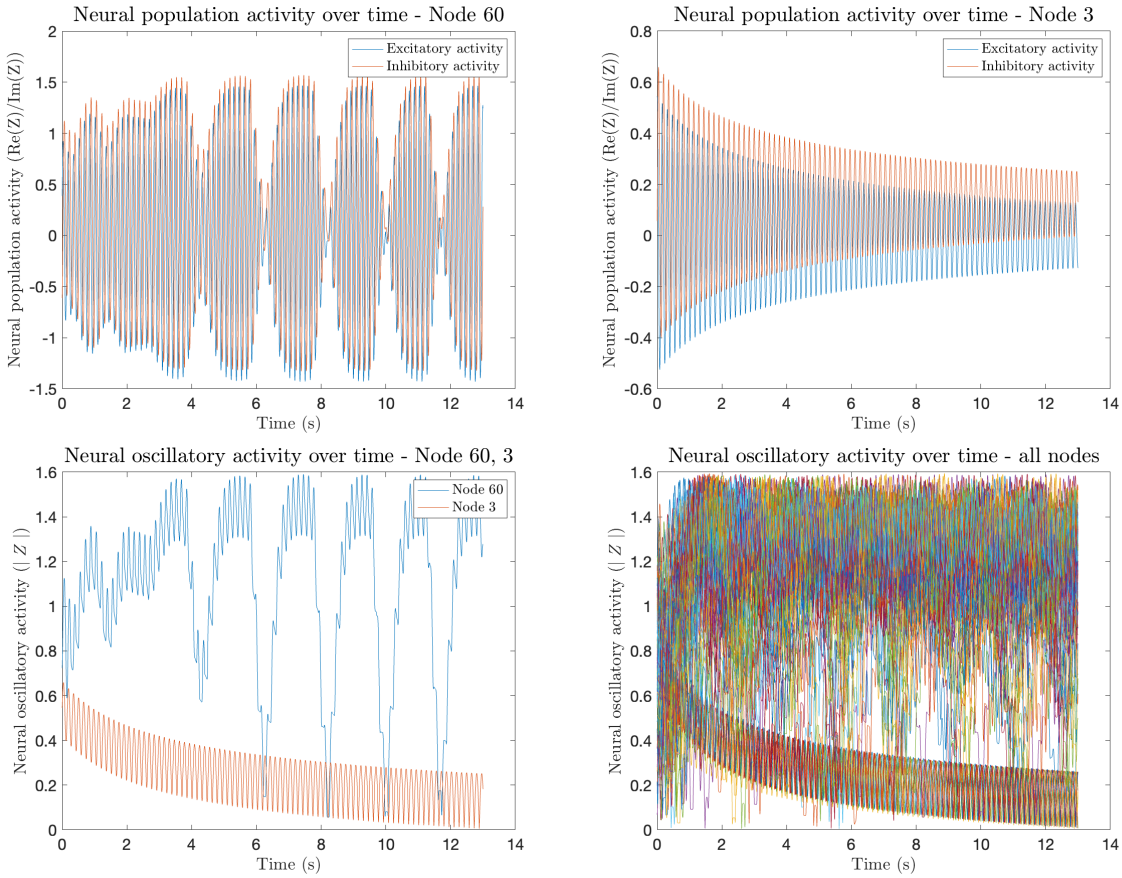

Fig. 5. Visualising the resting brain activity at a fixed year $T = 7$. The top-left and top-right figures show both the excitatory and inhibitory activity of two arbitrary nodes, one connected to its neighbours (left, Node 60) and one disconnected from neighbours (right, Node 3). The bottom-left figure shows the overall amplitude of oscillations ($|z|$) for both these example nodes over time; note in particular the disconnected Node 3 decays in absolute activity over time. The bottom-right panel shows the same absolute quantity for all nodes in the population.

show the absolute values of oscillatory activity (measured through $|z|$) for them both, reinforcing these trends. Finally, the bottom-right panel shows the same activity across all 83 nodes. All the disconnected nodes are represented by the declining trends, whereas all other nodes maintain continuous oscillatory activity.

Global cognitive decline after physical damage

As per Goriely and colleagues [5] we provide some summary measure of the resting state brain biological activity. To do this, the paper introduces three biomarkers:

- The overall power in the Gamma range $P(T) = \int_\Gamma PSD(\langle z \rangle)(\Omega) d\Omega$, where PSD is the power spectral density of the signal $\langle z \rangle = N^{-1} \sum_{j=1}^{N} \Re(z_j)$.
- The average oscillatory activity $A(T) = N^{-1} \sum_{j=1}^{N} t_{sim}^{-1} \int_0^{t_{sim}} |z_j(t)| dt$.
- The metastability index $B(T) = N^{-1} \sum_{j=1}^{N} \sigma_t^2(|z_j(t)|)$ where σ_t^2 is the variance of the signal over time interval $[0, t_{sim}]$.

Each of these biomarkers are calculated as the average over the entire brain $(P(T), A(T), B(T))$ but could also be calculated as an average over a particular region s $(P_s(T), A_s(T), B_s(T))$. For each case, we calculated the biomarkers for each year $T = [1, ..., 30]$, each repeated 12 times. The progression of the biomarkers with associated standard error bars is shown in Figure 6.

As can be seen, each biomarker declines over time, in particular from the 15th year onward. This is true also for each subregion of the brain.

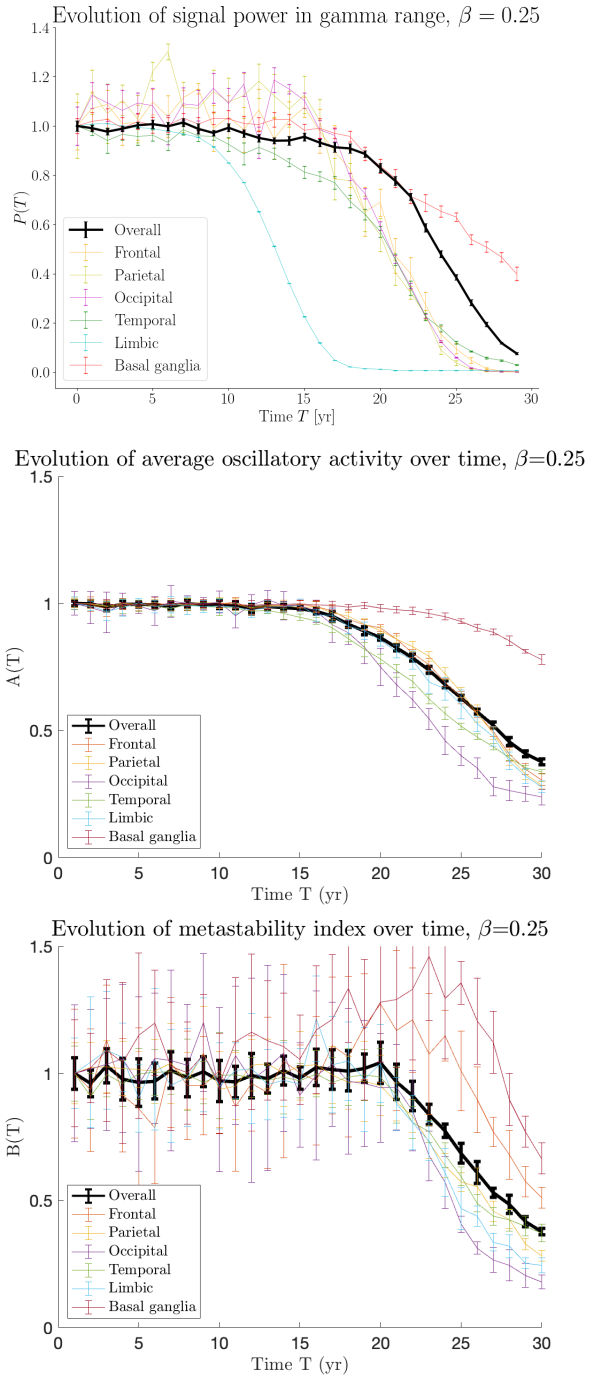

Fig. 6. Progression of each biomarker over time, for the overall brain and subregions. In each case, the trend is normalised against the value of the biomarker at $T = 1$ to ensure the relative decline can be observed.

Adaptation slows decline

In the previous section, we took as given the updated brain network at each time step T and computed the biomarkers. However, it is plausible that the brain does not just take the damage as given and could instead adapt its functioning to the damage.

To capture this effect, Goriely et al [5] proposes that the weight matrix is "re-weighted" to re-scale the connections between the nodes. Given an adaptation parameter ξ, we let the weight matrix evolve according to:

$$\bar{\mathbf{W}}(T) = \left[(1-\xi) + \xi\left(\frac{||\bar{\mathbf{W}}(T-1)||}{||\mathbf{W}(T||)}\right)\right]\mathbf{W}(T), \tag{6}$$

Where $\bar{\mathbf{W}}(0) = \mathbf{W}(0)$, and $||\mathbf{W}|| = \frac{1}{N^2}\sum_{jk} w_{jk}$ as earlier in the text. To see the effect of this change, note that if $||\mathbf{W}(T)|| < ||\bar{\mathbf{W}}(T-1)||$, then the weights are upscaled by a factor proportional to ξ. When $\xi = 1$, they are totally upscaled to ensure the mean connectivity does not decline at all. When $\xi = 0$, there is no rescaling and we have our previous result. For intermediate quantities the rescaling is partial.

The results can be seen in Figure 7, where we plot the decline in $A(T)$ (global oscillatory activity) and $A_s(T)$ (temporal lobe oscillatory activity). As expected, when the adaptation is high ($\xi = 1$) we observe little to no decline in the oscillatory activity, but as it decreases we see a quick return of the decline, albeit at varying levels of severity.

As noted in the paper, even with complete adaptation, there is some nonzero decline in the temporal oscillatory activity. This alludes to the fact that although the mean connection weight stayed the same, some qualitative shift in the pattern of connections in $\mathbf{W}(T)$ must have occurred, leading to a change in function. We explore this idea much more fully in the first extension to the work of [5] - examining topological changes in the brain network.

Extension 1

Topological evolution of the brain network

In this extension, we explore the question of not just how the connectivity of the brain network changes over the lifetime, but how the pattern of its connections (i.e. its topology) changes also.

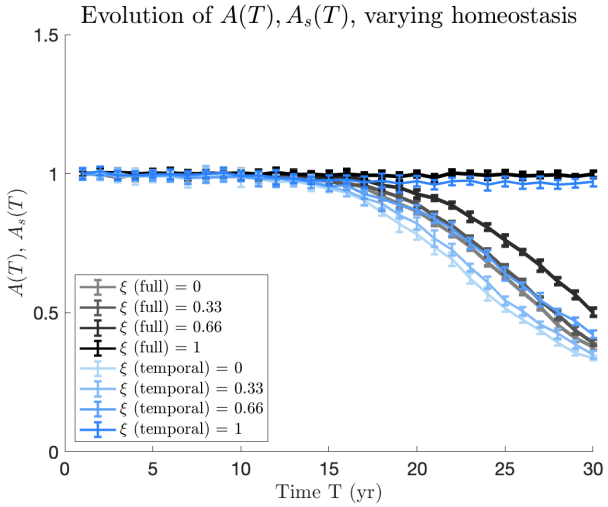

Fig. 7. Oscillation amplitude loss is less severe when we have adaption. For each time $T = [1...30]$, the biomarkers $A(T)$ (global oscillatory activity) and $A_s(T)$ (temporal lobe oscillatory activity) were measured from 12 runs of the simulation, for $\xi \in [0, 0.33, 0.66, 1]$. The raw biomarkers normalized against their initial value to observe the trend more clearly. As ξ increases, the decline in oscillatory activity becomes less severe. (Note that in the paper there is a typo - they show for no adaptation the highest recovery, and vice versa - the ξ labels were reversed).

Part 1: Identifying topological change

To motivate this, let us first note that in the original study, the primary metric used to measure connectivity in the network was $W(T)$. What was shown was that, predictably, as the damage spreads through the brain network and the weights between regions decayed, this connectivity measure decayed towards 0. This captures the overall trend of the connectivity, but arguably misses more subtle changes.

In order to illustrate this, consider Figure 8. Here, we compute for each node the total connectivity $d_j(T)$:

$$d_j(T) = \sum_{k=1}^{N} w_{jk}(T) \tag{7}$$

On the left hand side figure we show this quantity over time for each node, for three levels of damage $\beta = 0, 0.25, 1$. Consider also the mean of this quantity $\bar{d}(T)$:

$$\bar{d}(T) = \sum_{j=1}^{N} \frac{d_j(T)}{N} \tag{8}$$

This is superimposed on the figures as a thick red line. As can be clearly seen, for $\beta = 0$ (no damage), there is no decay in this mean node connectivity. For $\beta = 0.25$ (medium damage), there is some decay in the mean node connectivity, For $\beta = 1$ (large damage), there is very quick decay in the mean node connectivity. So far, this merely reinforces the existing result that $W(T)$ decays more quickly for a larger β[1].

However a critical question is whether the different node connectivity decays at the same rate. For example, one might think that nodes that are near the initial tau protein seeds (in the entorhinal region) might have their weights decay more quickly due to earlier buildup of damage, or perhaps nodes that are more central to the flow network decay more quickly, etc. In any case, we should see this reflected in the change in the *relative* connectivity of different regions. In order to visualise this, we plot instead of $d_i(T)$, the level of connectivity relative to the mean at that time step, $\frac{d_i(T)}{\bar{d}(T)}$. This is shown on the right hand side.

From here we see a very interesting picture. For $\beta = 0$, since there is no change in connectivity the relative connectivity does not change either. For $\beta = 0.25$, we see that the relative node connectivity stays fairly fixed. That is, all the nodes are decaying in their connectivity at pretty much the same fixed rate. However for $\beta = 1$, we can see that the relative connectivity of different nodes is changing - some are decaying faster (with a downward trend in the relative connectivity), whereas some get relatively *more* connected (with an upward trend).

We repeated the same analysis of the edge weights ($w_{jk}(T)$) and retrieved the same results - for $\beta = 0, 0.25$ the relative edge weights stayed constant, but for $\beta = 1$, the relative edge weights changed quite heavily over the lifetime (figures excluded for brevity - they look functionally identical to the relative changes for node connectivity).

[1] Since $\bar{d}(T) \propto W(T)$, this is to be expected.

We refer to this change in the relative connection strengths as *topological* changes in the brain network. This is meant to emphasize that not only is the magnitude of the flows between brain regions changing, the fundamental *pattern* of flows is changing. An analogy here might be road networks: if all the roads in a network lost a lane, the pattern of traffic flow will remain similar, with uniform slowing down on all roads. But if some roads lose many lanes and some roads lose very few, then we might expect traffic to reroute around the network. Similarly, the change in the relative connection strength between brain regions is a qualitatively different change to if all connections went down at once.

This leads us to our first conclusion:

- For no damage ($\beta = 0$), there is no change in connectivity or topology
- For medium damage ($\beta = 0.25$), there is change in connectivity but no change in topology
- For large damage ($\beta = 1$), there is change in both connectivity and topology

Part 2: Summary measures of topology
So far we have identified the topological changes by observing relative changes across the nodes and edges of the brain network. A sensible question to ask here is whether there exists any *summary* measures of topological change.

In order to find one we looked to the field of network science. One common approach to understand the topology of a network is to measure the "algebraic connectivity" of the graph, which is the second-smallest eigenvalue of the Normalised Laplacian[2]. We refer to it as $\lambda_2(T)$. The algebraic connectivity is used to study properties of robustness and synchronizability in networks. Networks that have a higher algebraic connectivity are more likely to be able to synchronize. Intuitively, networks that have low algebraic connectivity can be more easily split up into components that do not communicate strongly with each other. In contrast, networks that have higher algebraic connectivity are better integrated across the different subregions.

[2] We define the Normalised Laplacian $\mathbf{N} = \mathbf{D}^{-1/2}(\mathbf{D} - \mathbf{W})\mathbf{D}^{-1/2}$, where $\mathbf{D}$ is a diagonal matrix with $\mathbf{D}_{jj} = d_j$.

In Figure 9, we visualise how $\lambda_2(T)$ changes over time for different damage levels β. As can be seen, the greater the damage, the more quickly algebraic connectivity is lost. It should be noted in absolute terms, the overall drop is not huge (a fall of around 10% with $\beta = 1$). Still, it is enough to indicate that the topology is indeed changing in a measurable way as β increases.

Part 3: Implications for function
We have shown that the level of damage affects how the topology of the brain network changes, encouraging it to become less integrated and synchronisable. The remaining question here is how this might translate to real differences in brain function.

In order to do this we turn our attention to an area of neuroscience research called Integrated Information Theory (IIT). IIT posits that consciousness arising from the brain may be concretely measured with a quantity called Φ, a measure of how well the system integrates information between its subcomponents [10]. Much debate surrounds IIT [11], and though it may not provide a complete model of consciousness, it may offer a mathematical framework to model associated properties. Of particular note to us is the fact that it indicates that a less integrated brain network might lead to measurably different changes in consciousness under the definition they advocate. It stands to reason that perhaps this degeneration in the integration of the brain as identified by the algebraic connectivity might translate to changes in Φ, and provides a link between conciousness and the analysis of Alzheimer's explored in the original paper.

Notably AD is associated with impaired forms of consciousness such as syncope (transient loss of consciousness) and reduced levels of self-awareness [12]: both in the context of an individuals lack of recognition of their declining cognitive capacities (anosognosia), and more general cognizance of their thought processes (metacognition) [13]. Theories explaining these forms of cognitive decline in AD are currently insufficient beyond pointing to damage and reduced activity in a range of associated lobes such as the anterior cingulate cortex and inferior frontal gyrus [13]. Therefore, modeling levels of integrated

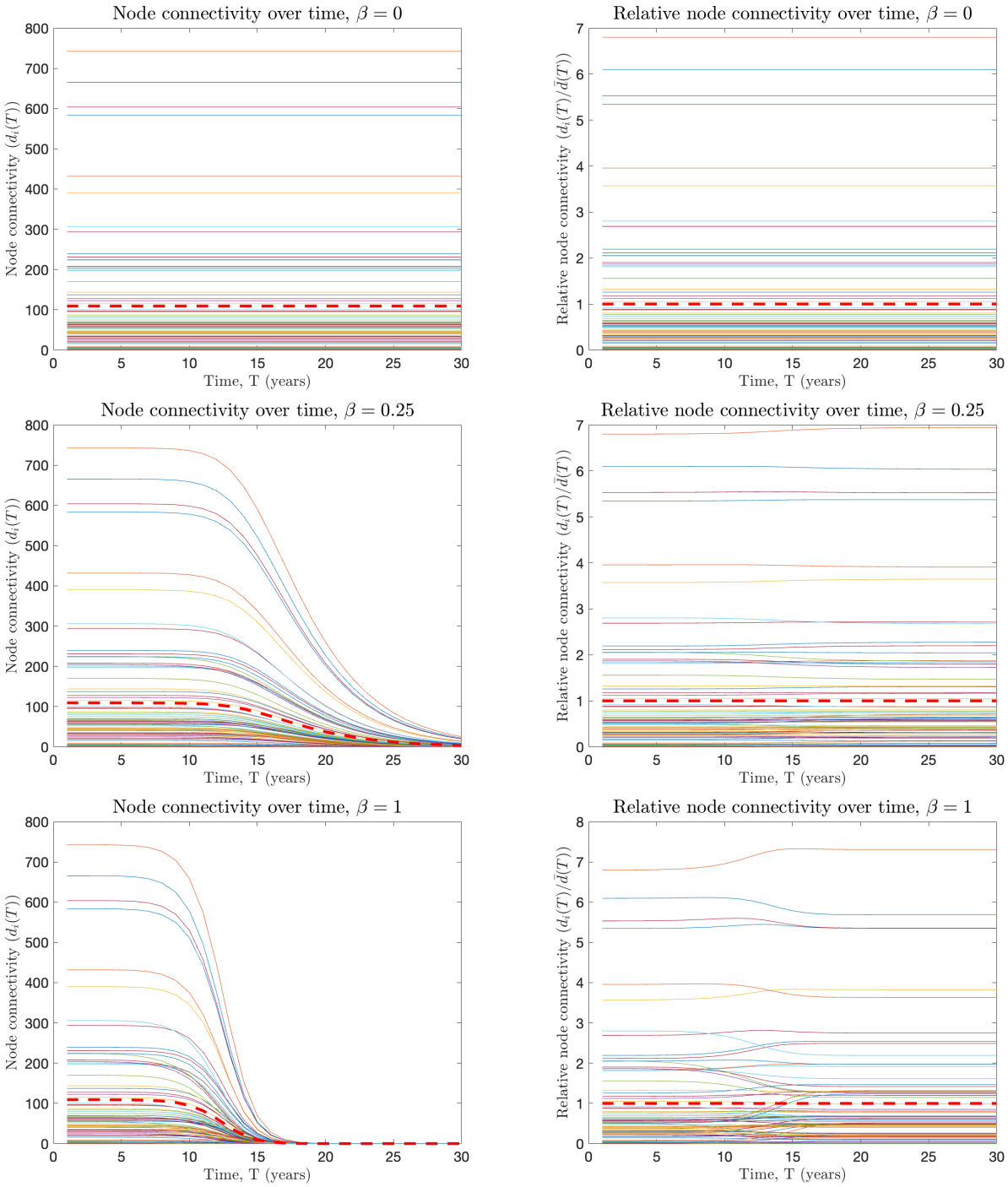

Fig. 8. We visualise how the overall connectivity of each brain region decays for $\beta = 0$ (top), $\beta = 0.25$ (middle) and $\beta = 1$ (bottom). The left hand plots show the overall connectivity of each node ($d_i = \sum_{j=1}^{N} w_{ij}$) at each time T. The mean connectivity $\bar{d} = \frac{\sum_i d_i}{N}$ is shown with a thick red line. The right hand plots show the relative connectivity of each node instead ($\frac{d_i}{\bar{d}}$).

information depending on the damage of brain regions, may provide a connectivity-based explanation for reductions in consciousness or related forms of self-awareness.

In order to do this we need to measure Φ in our network. There are numerous proposed measures of Φ in the literature, but for our purposes we rely on the definition provided by [14]. For any measure of Φ, the brain

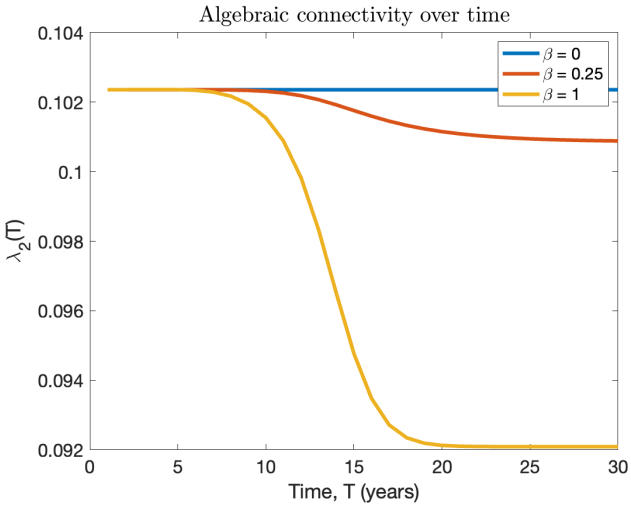

Fig. 9. Illustrating how the algebraic connectivity of the brain network decays over time, for different levels of degeneration $\beta = 0, 0.25, 1$. The greater the degeneration, the bigger the fall in algebraic connectivity.

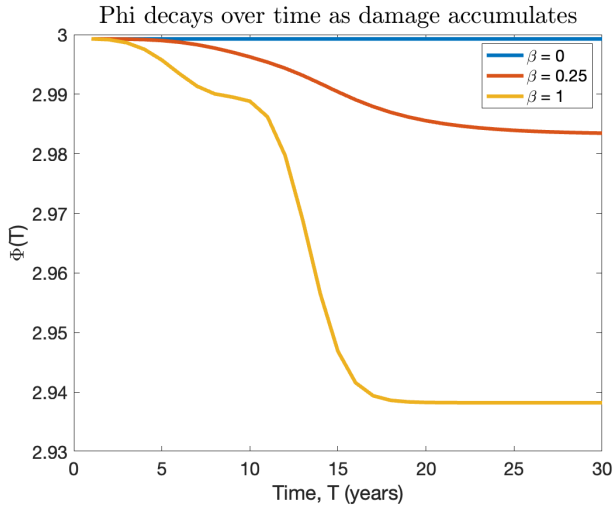

Fig. 10. The evolution of $\Phi(T)$ over time, for different levels of degeneration $\beta = 0, 0.25, 1$. The greater the degeneration, the bigger the fall in Φ, implying a lower measure of consciousness.

network needs to be divided into a "partition" $\mathcal{P}_r$ representing the r distinct modules that might communicate with one another. For some partition $\mathcal{P}_r$, they define Φ as:

$$\Phi_{\mathcal{P}_r} = \frac{1}{2} \log \left(\frac{\prod_{k=1}^{r} \det(\Sigma(M_t^k | M_{t+1}^k)}{\det(\Sigma(X_t | X_{t+1}))} \right) \quad (9)$$

Where X_t and M_t represent the state at time t of a random variable over the whole brain and partitions respectively, and X_{t+1} and M_{t+1} represent those variables after the system has integrated the information through some aggregation mechanism (the full details are provided in [14]). The choice of the partition matters here. In the paper, they choose the "maximum information partition", which is to treat each node as its own partition. This simplifies the calculation considerably. Furthermore, since each node in our data represents a parent region over sub-units of the brain, this method extended well to our analysis, so we adopted this approach. Using this, we were able to calculate $\Phi(T)$ for all times for our brain network, and the results are shown in Figure 10.

As can be seen, the greater the degeneration in the brain networks (β), the more the level of Φ drops. Interestingly, the drop mirrors very closely the change in the algebraic connectivity (Figure 9), suggesting the difference is indeed due to topological changes rather than changes in the absolute level of connectivity. It should also be noted that while the absolute change is not huge (representing a drop of 2%), even a small drop in a measure of consciousness might be considered noteworthy, and at the very least indicative of a possible link between brain degeneration, Alzheimer's and a formal notion of consciousness.

Extension 2

Delay times weighted by myelin thickness

In the original study, delay times were only affected by the length of the neural fibre. However, the speed of the signal per unit volume passing through an axon and the rate of material flow are significantly affected by the thickness of the surrounding myelin layer. Therefore, we wanted to investigate to what extent this factor changes the time variation of the parameters of each area. From the available connectome data, we were able to infer the myelin thickness of each neuronal pathway from the fractional anisotropy (FA). Namely, it describes the signal absorption capacity of a given tissue during a test. This parameter depends, among other things, on the number of fibres and the cross-sectional area of the myelin layer [15]. From previous studies, we know that there is an almost logarithmic relationship between

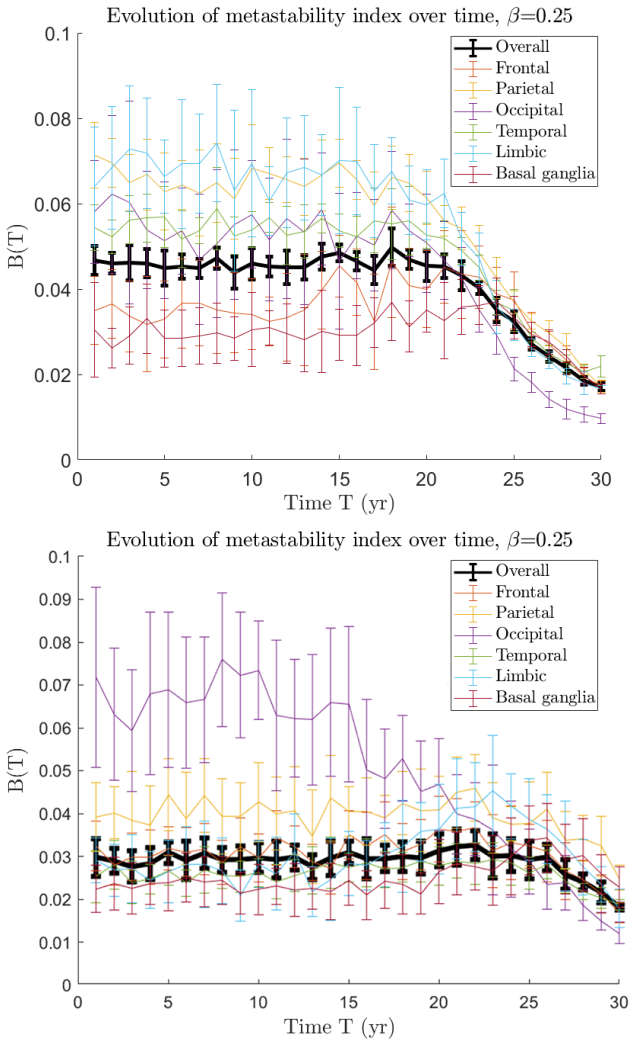

Fig. 11. Evolution of metastability index with (top) and without (bottom) weighting the delay times by myelin thickness.

myelin thickness and signal propagation speed [16]. Therefore, we weighted the existing delay times according to the following equation:

$$\tau_{kj} = \frac{d_{kj}}{150} \frac{1.5 \ln(f_{kj} + 0.2) + 5}{10} \qquad (10)$$

Where d_{kj} is the distance between the two nodes and f_{kj} is the FA between two nodes. Constant terms were chosen to replicate the exact curve provided in the paper [16].

The resulting A(T) diagram (average oscillatory activity) shows no significant difference between FA weighted and unweighted oscillation values. This may be explained by the fact that although myelin thickness affects the signal amplitude [17], excessive firing is observed near the plaques when some neuron layers are damaged, while the opposite is observed away from them [6]. These two processes can balance each other out, so the frequency change due to myelin thickness alone is not significant.

However, if we look at the change in metastability indices ($B(T)$, pictured in Figure 11), we can observe that there were large differences between the two conditions, both in the extent and the speed of deterioration due to degenerative processes. Among regions, the occipital cortex experiences the most significant extent and speed of deterioration from its initial value. This is a realistic result, as this area has one of the highest metabolic energy demands and also shows strong deterioration in AD, especially in the case of dementia [18].

Conclusion

Alzheimer's is a progressive neurodegenerative condition, known to be related to a continuous increase of toxic proteins in neurons. To date, there are computational models in existence that aim to explain the link between AD and its symptoms, as an effect of toxic proteins manifesting in the limbic region, followed by a generalised spread of the damage over the entire cortex. AD symptoms such as the reduction of gamma-range activity, oscillatory activity or metastability index, are apparent years after the onset of the damage. In this study, we replicated these base results and offered two interesting extensions. We first showed that the degeneration is uneven, leading to topological changes in the connectivity structure of the brain, in a manner that allows us to draw links to theories of decline in consciousness. Secondly, we modelled a more biologically plausible delay mechanism than in the base model, and found this was able to better explain deterioration in specific subregions that are closely linked to dementia.

For future work it would be important to extend this biological realism to various subsets of the computational model. For example, replacing the Wilson-Cowan resting brain state dynamics with models such as Stuart-Landau that have clearer biological interpretations of their parameters. This would allow us to build stronger confidence in

the results, and perhaps better model a wider range of neurodegenerative disorders.

Acknowledgments

The authors thank Stephen Coombes for all his help and valuable suggestions.

References

1. Marta Crous-Bou, Carolina Minguillón, Nina Gramunt, and José Luis Molinuevo. Alzheimer's disease prevention: from risk factors to early intervention. *Alzheimer's research & therapy*, 9(1):1–9, 2017.
2. Ron Brookmeyer, Elizabeth Johnson, Kathryn Ziegler-Graham, and H Michael Arrighi. Forecasting the global burden of alzheimer's disease. *Alzheimer's & dementia*, 3(3):186–191, 2007.
3. David L Felten, M Kerry O'Banion, and Mary E Maida. *Netter's atlas of neuroscience*. Elsevier Health Sciences, 2015.
4. Amelie Schäfer, Pavanjit Chaggar, Travis B Thompson, Alain Goriely, Ellen Kuhl, Alzheimer's Disease Neuroimaging Initiative, et al. Predicting brain atrophy from tau pathology: A summary of clinical findings and their translation into personalized models. *Brain Multiphysics*, 2:100039, 2021.
5. Alain Goriely, Ellen Kuhl, and Christian Bick. Neuronal oscillations on evolving networks: Dynamics, damage, degradation, decline, dementia, and death. *Physical review letters*, 125(12):128102, 2020.
6. Alexandra S Klein, José R Donoso, Richard Kempter, Dietmar Schmitz, and Prateep Beed. Early cortical changes in gamma oscillations in alzheimer's disease. *Frontiers in systems neuroscience*, 10:83, 2016.
7. Artemis Traikapi and Nikos Konstantinou. Gamma oscillations in alzheimer's disease and their potential therapeutic role. *Frontiers in Systems Neuroscience*, 15, 2021.
8. Jennifer A. McNab, Brian L. Edlow, and Thomas Witzel. The human connectome project and beyond: Initial applications of 300 mt/m gradients. *NeuroImage*, 80:234–245, 10 2013.
9. Sveva Fornari, Amelie Schäfer, Mathias Jucker, Alain Goriely, and Ellen Kuhl. Prion-like spreading of alzheimer's disease within the brain's connectome. *Journal of the Royal Society Interface*, 16(159):20190356, 2019.
10. Giulio Tononi, Melanie Boly, Marcello Massimini, and Christof Koch. Integrated information theory: from consciousness to its physical substrate. *Nature Reviews Neuroscience*, 17(7):450–461, 2016.
11. Michael A Cerullo. The problem with phi: a critique of integrated information theory. *PLoS computational biology*, 11(9):e1004286, 2015.
12. Eric Salmon, Perrine Ruby, Daniela Perani, Elke Kalbe, Steven Laureys, Stephane Adam, and Fabienne Collette. Two aspects of impaired consciousness in alzheimer's disease. *Progress in brain research*, 150:287–298, 2005.
13. Brendan Hallam, Justin Chan, Sergi Gonzalez Costafreda, Rohan Bhome, and Jonathan Huntley. What are the neural correlates of meta-cognition and anosognosia in alzheimer's disease? a systematic review. *Neurobiology of aging*, 94:250–264, 2020.
14. Xerxes D Arsiwalla and Paul FMJ Verschure. The global dynamical complexity of the human brain network. *Applied network science*, 1(1):1–13, 2016.
15. Noam Shemesh. Axon diameters and myelin content modulate microscopic fractional anisotropy at short diffusion times in fixed rat spinal cord. *Frontiers in Physics*, 6:49, 2018.
16. Taylor Chomiak and Bin Hu. What is the optimal value of the g-ratio for myelinated fibers in the rat cns? a theoretical approach. *PloS one*, 4(11):e7754, 2009.
17. Ehsan Shokri-Kojori, Dardo Tomasi, Babak Alipanahi, Corinde E Wiers, Gene-Jack Wang, and Nora D Volkow. Correspondence between cerebral glucose metabolism and bold reveals relative power and cost in human brain. *Nature communications*, 10(1):1–12, 2019.
18. Keneilwe Malomo and Ontefetse Ntlholang. Biparieto-occipital variant of alzheimer's dementia: Visual and praxis deficits. *J Psychol*, 2(2):1–2, 2018.